BBA - Molecular Basis of Disease 1865 (2019) 2111–2124

Contents lists available at ScienceDirect

BBA - Molecular Basis of Disease

journal homepage: www.elsevier.com/locate/bbadis

MICAL2 is expressed in cancer associated neo-angiogenic capillary endothelia and it is required for endothelial cell viability, motility and VEGF response

Ivana Barravecchia[a,b], Sara Mariotti[a], Angela Pucci[c], Francesca Scebba[a], Chiara De Cesari[a], Silvio Bicciato[d], Enrico Tagliafico[d], Elena Tenedini[d], Carla Vindigni[e], Marco Cecchini[f], Gabriele Berti[a,b], Marianna Vitiello[g], Laura Poliseno[g], Chiara Maria Mazzanti[h], Debora Angeloni[a,*]

[a] Scuola Superiore Sant'Anna, Institute of Life Sciences, 56124 Pisa, Italy
[b] University of Pisa, Pisa, Italy
[c] U.O.C. Anatomia Patologica, Azienda Ospedaliera Universitaria Pisana, 56100 Pisa, Italy
[d] Center for Genome Research, University of Modena and Reggio Emilia, 41125 Modena, Italy
[e] U.O.C. Anatomia Patologica, Azienda Ospedaliera Universitaria Senese, Policlinico Le Scotte, 53100 Siena, Italy
[f] Institute of Nanoscience, National Research Council, 56127 Pisa, Italy
[g] Oncogenomics Unit, Core Research Laboratory, ISPRO, Institute of Clinical Physiology, National Research Council, 56124 Pisa, Italy
[h] Fondazione Pisana per la Scienza, 56100 Pisa, Italy

ARTICLE INFO

Keywords:
MICAL2
neo-angiogenesis
Glioblastoma
Cardiac myxoma
Inflammation
CCG-1423

ABSTRACT

The capacity of inducing angiogenesis is a recognized hallmark of cancer cells. The cancer microenvironment, characterized by hypoxia and inflammatory signals, promotes proliferation, migration and activation of quiescent endothelial cells (EC) from surrounding vascular network. Current anti-angiogenic drugs present side effects, temporary efficacy, and issues of primary resistance, thereby calling for the identification of new therapeutic targets.

MICALs are a unique family of redox enzymes that destabilize F-actin in cytoskeletal dynamics. MICAL2 mediates Semaphorin3A-NRP2 response to VEGFR1 in rat ECs. MICAL2 also enters the p130Cas interactome in response to VEGF in HUVEC. Previously, we showed that MICAL2 is overexpressed in metastatic cancer. A small-molecule inhibitor of MICAL2 exists (CCG-1423).

Here we report that 1) MICAL2 is expressed in neo-angiogenic ECs in human solid tumors (kidney and breast carcinoma, glioblastoma and cardiac myxoma, $n = 67$, were analyzed with immunohistochemistry) and in animal models of ischemia/inflammation neo-angiogenesis, but not in normal capillary bed; 2) MICAL2 protein pharmacological inhibition (CCG-1423) or gene KD reduce EC viability and functional performance; 3) MICAL2 KD disables ECs response to VEGF *in vitro*. Whole-genome gene expression profiling reveals MICAL2 involvement in angiogenesis and vascular development pathways.

Based on these results, we propose that MICAL2 expression in ECs participates to inflammation-induced neo-

Abbreviations: AOU, Azienda Ospedaliera Universitaria; BP, biological processes; CCRCC, clear cell renal cell carcinoma; CTR, control, cells transfected with control plasmid; EC, endothelial cell; FBS, fetal bovine serum; FC, fold-change; FDR, false discovery rate; FFPE, formalin-fixed and paraffin-embedded; GO, Gene Ontology; GSEA, Gene Set Enrichment analysis; HMEC-1, Human Microvascular Endothelial Cells-1; HUVEC, Human umbilical vein endothelial cells; KD, knock-down; LAD, left descending anterior artery; M2KD, MICAL2 KD; M3KD, MICAL3 KD; MICAL, molecule interacting with CasL; MTT, 3-(4,5-Dimethylthiazol-2-yl)-2,5-diphenyltetrazolium bromide; NES, normalized enrichment score; qRT-PCR, Real-Time Quantitative Reverse Transcription polymerase chain reaction; TFA, tube formation assay; VEGF, vascular endothelial growth factor; VEGFR1, vascular endothelial growth factor receptor 1; WHA, wound healing assay; VSMC, vascular smooth muscle cells; WT, wild-type

* Corresponding author at: Scuola Superiore Sant'Anna, Institute of Life Sciences, Via G. Moruzzi, 1, 56124 Pisa, Italy.
E-mail addresses: ivana.barravecchia@santannapisa.it (I. Barravecchia), f.scebba@santannapisa.it (F. Scebba), c.decesari@santannapisa.it (C. De Cesari), silvio.bicciato@unimore.it (S. Bicciato), tagliafico.enrico@unimore.it (E. Tagliafico), elena.tenedini@unimore.it (E. Tenedini), marco.cecchini@nano.cnr.it (M. Cecchini), g.berti@santannapisa.it (G. Berti), mvitiello@ifc.cnr.it (M. Vitiello), c.mazzanti@fpscience.it (C.M. Mazzanti), angeloni@santannapisa.it (D. Angeloni).

https://doi.org/10.1016/j.bbadis.2019.04.008
Received 29 October 2018; Received in revised form 31 March 2019; Accepted 11 April 2019
Available online 18 April 2019
0925-4439/

angiogenesis and that MICAL2 inhibition should be tested in cancer- and noncancer-associated neo-angiogenesis, where chronic inflammation represents a relevant pathophysiological mechanism.

1. Introduction

Like normal tissues, malignant tissues require supply of oxygen and nutrients and removal of metabolic waste products to strive and survive. The formation of new blood vessels satisfies this need and accompanies the development of clinically relevant tumors, to the extent that the capacity of inducing angiogenesis is a recognized hallmark of cancer cells [1].

Growth factors and chemokines chaotically released by cancer cells in the niche of solid tumor promote proliferation, migration and tube formation of quiescent endothelial cells (ECs) from surrounding vascular network. Tumor-associated blood vessels and their endothelial lining derive, in essence, from the vasculature of normal, surrounding tissue. Although they are not part of the cancer clone, nevertheless their phenotype is abnormal in most of their aspects, from molecular to ultrastructural and functional [2,3]. Their formation leads to a hostile environment in which hypoxia, low pH, and high pressure of interstitial fluid come together to select malignant phenotype and facilitate the escape of tumor cells through leaky vessels [4], while the function of immune cells and the transport of chemotherapeutics are hampered.

The anti-angiogenic approach to treat cancer was first proposed by Judah Folkman [5] and now anti-angiogenic drugs, such as bevacizumab, sunitinib, and sorafenib are available for oncological patients [6]. The overall goal of the anti-angiogenic approach is to stabilize tumor growth through preventing the maturation of a functional vessel network, compromising the existing tumor-associated vasculature and inhibiting new vessel formation. Multiple tools, including antibodies, the inhibition of the tyrosine kinase activity of EC receptors and antisense strategy for down regulation of gene expression, have been used primarily against pro-angiogenic factors because of their leading role in the formation of new blood vessels, exploiting phenotypic characteristics of tumor-associated endothelium. Genes that are selectively overexpressed in blood vessels during tumor angiogenesis were identified, the molecular diversity of vasculature and vessel formation either in healthy organs or at disease sites representing the rational basis for a targeted diagnostic and therapeutic approach [2,7,8].

Despite anti-angiogenic drugs allow at times impressive clinical achievements in terms of tumor shrinkage and increased survival that can be measured in months, their benefits are temporary because inevitably the disease progresses again, not to mention that primary resistance remains a problem [9,10].

These observations call for a deeper understanding of the molecular distinctiveness of tumor blood vessels and for the identification of new therapeutic targets associated to neo-angiogenesis.

Molecule interacting with CasL 2 (MICAL2) belongs to a three-member family of multi-domain flavoprotein monooxygenase enzymes that catalyze actin oxidation-reduction reactions destabilizing F-actin in cytoskeletal dynamics [11–13]. Others and we showed that MICAL2 is over-expressed and it is a negative prognostic factor in aggressive human gastric and kidney ([14]; https://www.proteinatlas.org/ENSG00000133816-MICAL2/pathology/tissue/renal+cancer); prostate [15]; bladder [16], and breast [17] carcinomas. Recently, MICAL2 over-expression was linked to chemoresistance and increased mortality in endometrial cancer patients [18].

MICAL2 knock-down (KD) in kidney cancer cells had a profound impact on cell morphology, motility and invasive capacity, clearly causing mesenchymal to epithelial transition [14]. We also reported preliminarily that MICAL2 is expressed in cancer-associated capillaries [14].

MICAL2 is required to mediate Semaphorin3A-NRP2 response to VEGFR1 in rat ECs *in vitro* [19]. Further, VEGF promotes the assembly of p130Cas interactome that contains, among others, also the MICAL2 protein. Such interactome is responsible for driving chemotactic signaling and angiogenic properties of ECs [20].

On these bases, we investigated the role of MICAL2 in neo-angiogenic endothelium.

Herein we show that hampering MICAL2 activity in ECs, chemically or through gene KD, hinders their viability and functional properties reducing their ability to respond to VEGF stimulation. Transcriptome analysis of MICAL2 KD cells reveals a role of the gene in pro-angiogenic pathways, among others.

Altogether our observations point to MICAL2 as a possible new target for anti-angiogenic therapy.

2. Materials and methods

2.1. Tissue specimens

Histology was performed in all formalin-fixed and paraffin-embedded (FFPE) tumors entering this study and obtained from patients who underwent palliative or curative surgery. Histological slides were retrospectively and independently reviewed at the Department of Pathological Anatomy of AOU Senese, Siena, Italy (primary gastric, kidney and breast carcinoma and glioblastoma IDH1 wild-type) and AOU Pisana, Pisa, Italy (primary breast carcinoma, glioblastoma and cardiac myxoma) by experienced pathologists using standard criteria to assess histological diagnosis and grading.

2.2. Cell lines and culturing

HMEC-1 (Human Microvascular Endothelial Cells, CDC, Atlanta, GA USA) is an immortalized EC line derived from human dermal capillaries [21]. SVEC4–10 (ATTC; CRL-2181) is an immortalized mouse cell line derived from axillary lymph node ECs [22]. HMEC-1 cells were kept as in [23]. SVEC4–10 were grown in DMEM (Lonza) added with 10% fetal bovine serum (FBS, Gibco), 4 mM L-glutamine, 1.5 g/l sodium bicarbonate, 100 U/ml penicillin, 100 µg/ml streptomycin. Cell cultures were kept in 5% CO_2 incubator at 37 °C, and routinely tested for mycoplasma contamination (MycoAlert Kit, Lonza).

2.3. Rat models of pathological neo-angiogenesis

We used two different models of rat pathological neo-angiogenesis: the infarcted heart model and the model of myocardial ischemia and reperfusion.

Wistar male rats, 10–12 week old, 200–300 g average body weight, were used. Animals were anesthetized with a combination of Zoletil and Xilazine (respectively 50 mg and 3 mg per kg of body weight), intubated with oropharyngeal catheter and ventilated with a volume of 1.2 ml/100 g at the rate of 70 cycles per minute (min). Once stabilized, animals underwent left lateral thoracotomy at the fourth intercostal space. The pericardium was then translocated to expose the left descending anterior artery (LAD). The artery at the level of the first diagonal branch was wound with a 2 mm silk suture thread and then occluded for an average time of 40 min. After LAD ligature, the muscle layer and the skin were stitched up, the catheter removed, and the animal kept under observation for the next 4–6 h (hours).

In the myocardial infarction model, animals (n = 3) were sacrificed after one day. In the model of ischemia and reperfusion, animals (n = 3) were reperfused for a period of 3–7 days and finally sacrificed.

Two sham animals were used per each procedure. Subsequently, the hearts were removed and fixed in 10% formalin buffer for 24/48 h. Finally, the samples were dehydrated with increasing concentration ethanol series, xylene washed, paraffin included, and microtome cut.

2.4. Immunohistochemistry

Immunohistochemistry was performed as previously described [14] with avidin-biotin complex on FFPE sections of each tumor. Briefly, slides were deparaffinized, rehydrated and treated with H_2O_2 before incubation with primary (1:2500 or 1:500, rabbit polyclonal anti-MICAL2 generated in our laboratory, [14]) and secondary antibody (ABC Kit, Rabbit, Vectastain, Vector Laboratories) solutions, exposed to the chromogenic substrate (CN/DAB Substrate Kit, Thermo Scientific) and mounted in Canada Balm (Bioptika) after hematoxylin counter-staining.

2.5. RNA and cDNA preparation for RT-PCR and qRT-PCR

Total RNA was isolated with ReliaPrep RNA Cell Miniprep System (Promega). Purified total RNA samples were quantified at the spectrophotometer (NanoDrop ND-1000, NanoDrop Technologies), and quality-checked (Bioanalyzer 2100, Agilent Technologies). cDNA was synthesized using random hexamers and oligo-dT primers (QuantiTect Reverse Transcription Kit, Qiagen), in 2720 Thermal Cycler (Applied Biosystems, USA). QRT-PCR was performed in technical and biological triplicates, in ABI 7000 PRISM SDS thermal cycler (Applied Biosystems) and RotorGene (Corbett Research). Data were analyzed through relative quantification with the –ΔΔCt method. Primer sequences: Supplementary Table 1; 18S5 and actin-beta were the reference genes. PCR products were sequence-verified (3730 DNA Analyzer automated sequencer, Applied Biosystems). For qRT-PCR on SVEC4–10, TaqMan GeneSpecific Assays FAM dye-labeled and TaqMan Universal PCR Master Mix were used, mouse actin-beta was the reference gene (Applied Biosystems), Supplementary Table 1.

2.6. Gene silencing in endothelial cell lines

MICAL2 was knocked-down *in vitro* as in [14], see also legend to Supplementary Fig. 1. Mical3 was knocked-down similarly. The following nomenclature is used throughout the text: WT for wild-type, genetically untreated cells; M2KD for human MICAL2 KD cells (with different clonal populations of murine SVEC4–10 identified as KD, and of HMEC-1 identified as KD1 and KD2); M3KD for Mical3 KD cells; CTR for cells transfected with control plasmid.

2.7. Cell proliferation and viability assays

Cell proliferation was measured by manual counting (Trypan Blue exclusion assay, Sigma-Aldrich) on HMEC-1 cells exposed to 5 and 10 μM CCG-1423 (Sigma). Cell viability was measured with MTT assay (Sigma-Aldrich), reading samples at 590 nm (ETI-SYSTEM Fast Reader, Sorin Biomedica).

2.8. Cell staining

F-actin was stained with 488 Acti-stain (1:250, Cytoskeleton), in cells fixed with 2% paraformaldehyde (Sigma).

2.9. 2D cell adhesion, motility, angiogenesis and chemotaxis assays in vitro

Adhesion was evaluated according to standard protocols. 10,000 cells were plated in type-I collagen-coated (0.1 μg/μl, Sigma-Aldrich) vessels and challenged 60, 90 and 120 min afterwards, stained with crystal-violet solution and read at 590 nm (ETI System Fast Reader, Sorin Biomedica).

8-h wound healing assay (WHA) was performed on all cell lines, either practicing a scratch or using the Culture-Insert system (Ibidi), seeding 12,500 cells in each insert compartment. Assays were performed differently depending on drug under test (see Figure Legends).

The tube formation assay (TFA) was performed with 15,000 cell seeded on angiogenesis μ-slides (Ibidi) coated with Geltrex (Thermo Fisher Scientific).

2.10. Genome-wide gene expression profiling

For gene expression profiling, Affymetrix GeneChip Mouse Genome 430 2.0 Array (Affymetrix) was used. Total RNA was extracted using TriPure (Roche) from a pool of three independent RNA samples for each of the following: WT, CTR, M2KD and M3KD SVEC4-10 cells (the latter used as a comparison model, further data not shown). RNA quality and purity were assessed on the Agilent Bioanalyzer 2100 (Agilent Technologies); RNA concentration was determined using the NanoDrop ND-1000 Spectrophotometer (NanoDrop Technologies). RNA was then treated with DNaseI (Ambion). *In vitro* transcription, hybridization and biotin labeling were performed according to Affymetrix 3′IVT protocol (Affymetrix).

All microarray data analyses were performed in R (version 3.3.2) using Bioconductor libraries (BioC 3.1) and R statistical packages. Probe level signals were converted to expression values using the robust multi-array average procedure in the *rma* function of the Bioconductor *affy* package. Raw data are available at Gene Expression Omnibus under accession number GSE120494.

To identify genes associated with Mical2 silencing in SVEC4–10 cells, we compared the expression levels of cells as above using a criterion based on the fold change (FC). Briefly, we considered up and down regulated those genes with an absolute FC larger than a selected threshold (*e.g.* $\geq +1.7$) in the comparison of M2KD and WT cells and with an absolute FC lower than a selected threshold (*e.g.* ≤ -1.7) in the comparison of M2KD and WT cells, respectively.

Functional over-representation was performed using the Preranked tool of the Gene Set Enrichment Analysis (GSEA; http://software.broadinstitute.org/gsea/index.jsp) and the curated gene sets of the Molecular Signatures Database (MSigDB) derived from the Hallmark, Biocarta, KEGG, and Reactome pathway collections (http://software.broadinstitute.org/gsea/msigdb/collections.jsp). GSEAPreranked was applied on the FCs of M2KD up and down regulated genes. Prior to GSEA analysis, we converted mouse Entrez IDs into the corresponding human homologous genes using the HUGO Gene Nomenclature Committee (HGNC) database (https://www.genenames.org/cgi-bin/hcop). Gene sets were considered significantly enriched at false discovery rate (FDR) ≤ 0.25 when using Signal2Noise as metric and 1.000 permutations of gene sets. The dot plot, showing the most significantly activated pathways in the M2KD cells, was generated using the ggplot function of the ggplot2 R package.

Protein networks activated in Mical2 KD cells were identified using the StringApp (Search Tool for the Retrieval of Interacting Genes/Proteins) [24]. It builds the protein-protein interaction network by considering String 10 default interaction parameters. A medium confidence score of 0.4 was set as minimum required interaction score and all the disconnected nodes were removed. To explore the associations between M2KD deregulated genes on a global scale, several types of interactions were considered, including known experimental interactions and pathways, co-expression data, interactions from genomic data, co-occurrences of gene/proteins and interactions inferred from other organisms based on orthology.

Cytoscape (http://www.cytoscape.org/) was used to assign node colors based on gene expression level. The Network Analyzer, in Cytoscape, was used to generate node and edge style: node size was fixed according to betweenness centrality while the string combined score of interaction was considered to assign edges color and size. The ClusterOne algorithm, implemented in cytoscape, was used to detect

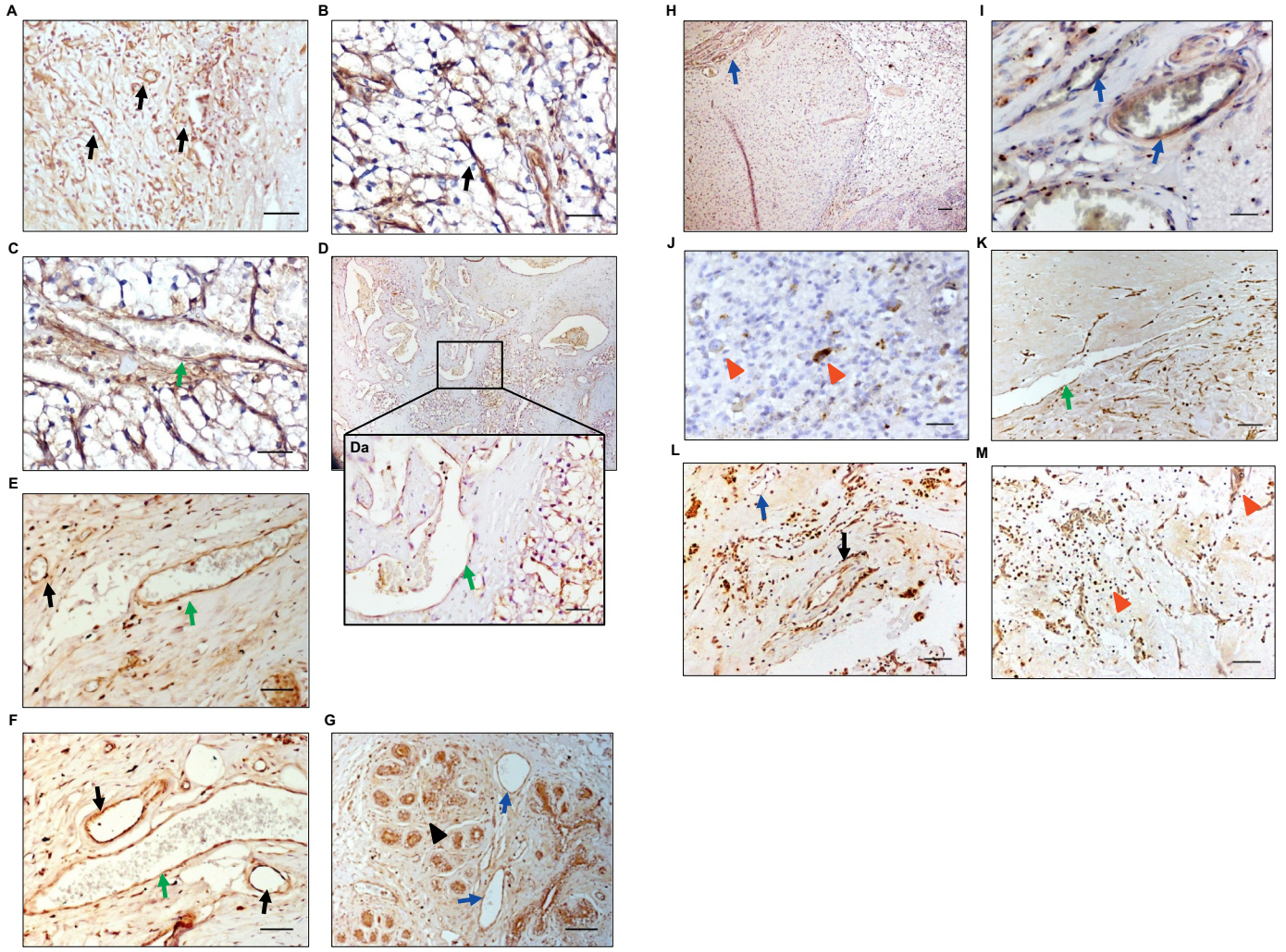

Fig. 1. MICAL2 is expressed by neo-angiogenic endothelium of gastric, kidney and breast carcinoma, glioblastoma, and cardiac myxoma.
Histopathology sections of diverse, highly vascularized, solid tumors were stained with polyclonal anti-MICAL2 antibody: 1:2500 in diffuse histotype gastric cancer (A); 1:1500 in clear cell renal cell carcinoma, CCRCC (B, C, D and Da); 1:500 in diffuse G3 breast cancer (E, F, G); 1: 1500 in IDH1 wild type glioblastoma (H, I, J); 1:500 in cardiac myxoma (K, L, M). With the exception of gastric cancer (A), tumor cells were not MICAL2 positive, whereas MICAL2 was found highly expressed in frank neo-angiogenic ECs (black arrows in A, B, E, F). Other ECs were also stained: ECs in markedly dilated vessels within the tumor mass (green arrows in C, Da, E, F, L) and seemingly activated ECs in vessels embedded in or very close to the tumor mass (blue arrows in G, H, I, K).
Black arrowheads: residual non-neoplastic mammary glands adjacent to cancer tissue (G); red arrowheads: inflammatory cell infiltrate (J, M). Pictures were taken with optical microscope (Olympus BX43) equipped with camera Olympus DV20 and CellSens Dimension software, Olympus (A, B, C, D, Da, E, F, G, L, M) and Nikon Eclipse equipped with NIS Elements D (J, K). Magnification: 5× in D, H, scale bar: 100 μm; 20× in A, B, C, E, F, G, K, L, M, scale bar: 50 μm; 40× in I, J, Da, scale bar: 10 μm.
Only samples containing 70–80% or more tumor cells and adjacent normal tissue were used (n = 67).

protein modules in the network by considering ClusterOne default parameters and String-combined scores as weight for the clustering. 150 proteins with at least one interaction form a main network among genes affected by M2KD.

2.11. In silico analysis

Public, web-based resources used for this study:
http://perlprimer.sourceforge.net/
https://www.ncbi.nlm.nih.gov/tools/primer-blast/
http://www.ncbi.nlm.nih.gov/unigene/,
http://www.cbs.dtu.dk/services/NetPhos/,
http://web.expasy.org/findmod/,
http://rsbweb.nih.gov/ij/index.html,
http://www.genesapiens.org/,
http://discover.nci.nih.gov/cellminer/analysis.do
https://david.ncifcrf.gov/
http://software.broadinstitute.org/gsea/index.jsp
http://software.broadinstitute.org/gsea/msigdb/collections.jsp
https://www.genenames.org/cgi-bin/hcop
http://www.cytoscape.org/
https://www.proteinatlas.org/ENSG00000133816-MICAL2/pathology/tissue/renal+cancer
EPD: https://epd.vital-it.ch/search_EPDnew.php?query=MICAL2&db=human
PROMO: http://alggen.lsi.upc.es/cgi-bin/promo_v3/promo/promoinit.cgi?dirDB=TF_8.3

3. Results

3.1. MICAL2 is expressed by the neo-angiogenic endothelium of different solid human tumors

Previously, we showed with immunohistochemistry the expression

of MICAL2 protein in ECs of neo-angiogenic capillaries branching off within the tumor mass of gastric and kidney carcinoma [14]. Expanding the range of observation, herein, we show MICAL2 immunoreactivity in ECs of numerous newly formed vessels, densely represented within gastric adenocarcinoma and clear cell renal cell carcinoma (CCRCC) (Fig. 1A, B) and in ECs of dilated vessels embedded in broad fibrotic bands of CCRCC (Fig. 1C, D). Both pre-formed and newly formed vessels were characterized by a thin wall without vascular smooth muscle cell (VSMC) layer and therefore morphologically distinct from arterioles. Further, in breast ductal carcinoma MICAL2 immunostaining was localized to the dilated vessels within the tumor and in the smaller, newly formed intra-tumoral vessels (Fig. 1E, F). In breast tissue, MICAL2 was detected in residual non-neoplastic mammary glands in close proximity of the tumor mass, mostly localized to basal myoepithelial cells and in adjacent thin vessels (Fig. 1G). In glioblastoma, MICAL2 was expressed in the vessels within the neoplastic mass, next to the invasive front (Fig. 1H, I). We also found polarized MICAL2 expression in cancer cells and in the inflammatory cells, mainly macrophages, associated with the neoplasia (Fig. 1J), with immunoreactivity eccentrically localized to the perinuclear cytoplasm. In cardiac myxoma, tumor cells were organized as perivascular cuffs or in cords/nests within the myxoid stroma, closely associated to the capillaries, which were abundant within the neoplasia and strongly positive for MICAL2 (Fig. 1K). MICAL2 was also expressed in the dilated vessels that are usually well represented at the periphery of the tumor mass (Fig. 1L). MICAL2 immunostaining was negative or very weak in the neoplastic cells, whereas it was intense in the inflammatory cells (macrophages and lymphocytes) that are abundant in this tumor (arrow in Fig. 1M).

Altogether, these findings show that within solid human tumors the neo-angiogenic vasculature comprises ECs and EC-looking cells that are strongly positive for MICAL2, regardless of the tumor histotype.

3.2. MICAL2 is expressed in endothelial cells of a pathophysiological model of neo-angiogenesis

To verify the hypothesis of an involvement of MICAL2 in neo-angiogenesis, we turned to a pathophysiological model of neo-angiogenesis different from cancer but equally prone to tissue inflammation and hypoxia. Specifically, we used rat models of myocardial infarction (Fig. 2A) and myocardial ischemia/reperfusion (Fig. 2B) because in such models ischemia activates a strong inflammatory response that share many aspects with tumors [25]. Cardiac myocytes in the healthy myocardium were strongly positive for MICAL2, unlike those in the central necrotic area (Fig. 2A, B, star), of course. In the ischemic zone, we found ECs strongly positive for MICAL2 immunoreaction in new capillaries (Fig. 2C) and in activated capillaries (Fig. 2D). The inflammatory cell infiltrate was also strongly positive (Fig. 2E, arrow). The endothelium of the pre-existing arterioles was MICAL2 negative in the ischemic zone. The VSMC layer of arterioles showed marked immunoreactivity (Fig. 2F). In the remote zone, capillary ECs were MICAL2 negative (Fig. 2G), while again, the protein was detected in the VSMC of large-caliber, pre-existing vessels (Fig. 2H), and in cardiomyocytes (Fig. 2I). In the border zone, at the edge between healthy and ischemic tissue, we found spotted staining, with some capillaries showing very low MICAL2 expression, mingled with others completely negative (Fig. 2J).

Overall, these results showed that the endothelium of neo-angiogenic vasculature, and more in general activated ECs forming capillaries next to a region of hypoxia and inflammation, feature strong MICAL2 expression, suggesting MICAL2 promoter proneness to inflammatory signals.

3.3. MICAL2 is a target of TNF-alpha. Direct inhibition of MICAL2 reduces functional properties of activated endothelial cells in vitro

Given the high immunoreactivity of MICAL2 at sites of tissue inflammation, we asked whether inflammatory cytokines drive MICAL2 expression. Accordingly, we stimulated human microvascular ECs (HMEC-1) with a key pro-inflammatory cytokine, human recombinant TNF-alpha (10 ng/ml, for 24 h). Expression of VCAM-1, an adhesion molecule whose increase represents a significant early event in inflammation, here analyzed for reference, increased over 1300 folds (Supplementary Fig. 2A). MICAL2 expression increased over 7 folds (Supplementary Fig. 2B).

Further, the stimulation with TNF-alpha determined an increase of bidimensional cell motility: cells treated with TNF-alpha in serum-free medium covered the same area as cells in complete medium (Supplementary Fig. 2C, D).

Moreover, as it was recently shown that CCG-1423, a small molecule that inhibits SRF/MRTF-A pathway, is a MICAL2 enzymatic activity inhibitor [32], we tested whether MICAL2 pharmacological inhibition might hamper EC functional properties. We found that 10 μM CCG-1423 caused a 70% proliferation reduction in treated cells (Fig. 3A). Functional properties of HMEC-1 cells were also affected, with 60% reduction of covered area in an 8-h WHA (Fig. 3B, C), and a marked reduction of several indicative parameters in a 24-h TFA (Fig. 3D–H).

Noticeably, the treatment with CCG-1423 overcomes the pro-inflammatory activity of TNF-alpha: an 8-h WHA with HMEC-1 cells pre-treated with TNF-alpha (10 μM) and exposed to CCG-1423 (10 μM, for 20 h), showed a 70% reduction of covered area (Fig. 3I, J) and, what is more, the specific MICAL2 inhibitor caused a complete containment of the cell motility response to TNF-alpha, as indicated by the absence of statistically significant difference between cells treated with CCG-1423 before and after exposure to TNF-alpha (Fig. 3I).

Altogether, these data suggest that the MICAL2 gene is a target of tissue inflammation. MICAL2 direct inhibition markedly reduced the effect of a powerful inflammatory cytokine and hampered functional properties of activated ECs *in vitro*.

3.4. MICAL2 knock-down in human and murine endothelial cells reduces cell viability and function and impairs the response to VEGF stimulation in vitro

We then explored the role of MICAL2 in ECs starting with a loss-of-function approach in two EC lines of capillary origin, human HMEC-1 and murine SVEC4–10. With species-specific shRNA strategy, we obtained mixed populations of knocked-down cells with around 40% (KD1 cells) and around 80% (KD2 cells) expression reduction in HMEC-1 (Supplementary Fig. 1A), and over 80% in SVEC4–10 (KD cells, Supplementary Fig. 1B).

Interestingly, MICAL2 gene KD (M2KD) did not interfere with MICAL1 or MICAL3 gene expression, which remained unchanged (Supplementary Fig. 1C, D).

M2KD reduced HMEC-1 (Fig. 4A) and SVEC4–10 cell viability (Fig. 4B) in statistically significant way. M2KD also impaired SVEC4–10 cell adhesion of about 50%, either on plastic (data not shown) or collagen I-treated plates (Fig. 4C), both at 90 and 120 min from plating. Next, we evaluated the effect of M2KD with TFA. In the presence of 10% FBS, WT and CTR cells established reciprocal contact and organized themselves in tubular structures (Fig. 4D). On the contrary, KD1 and KD2 cells failed to develop stable loops and tubes, forming only sparse nets if any at all (Fig. 4D).

Further, given the importance of VEGF signaling in angiogenesis, and also the well-known adverse collateral effects of anti-VEGF treatment in cancer, we explored more the relation between MICAL2 and VEGFR in our cell systems, also in light of the known interaction of MICAL2 with VEGFR1 to mediate rat EC response to Sema3A *in vitro* [19].

We characterized MICAL2 loss-of-function on VEGF-stimulation response in WHA *in vitro*. Motility of M2KD cells was markedly reduced compared to reference cells, (Fig. 5A and Supplementary Files ~~3~~ 4 and

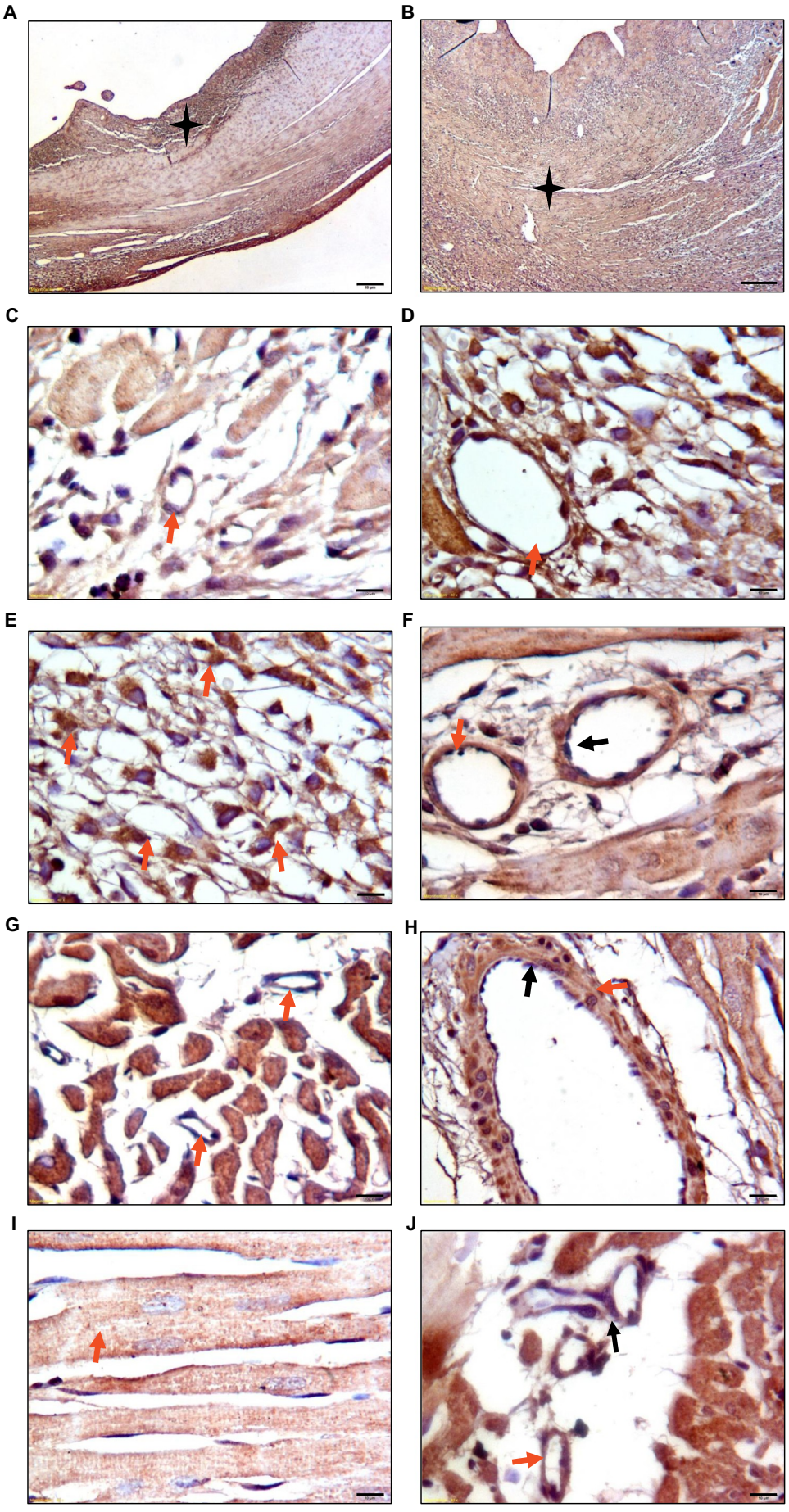

Fig. 2. Endothelial cells of blood vessels activated by tissues inflammation express MICAL2. Immunohistochemistry of rat myocardial infarcted (A) and ischemic/reperfused (B) heart tissues stained with anti-MICAL2 antibody (1:2500). Stars: healthy tissue. Red arrows: new capillaries were MICAL2 positive (C), MICAL2 positive ECs in activated capillaries next to the ischemic zone (D), inflammatory cell infiltrate in the ischemic zone (E), MICAL2 positive VSMC layer of arterioles in the remote zone (F, black arrow: MICAL2 negative ECs), MICAL2 negative ECs of the remote zone (G), MICAL2 positive VSMC layer of large-caliber, pre-existing arteriole (H, where ECs are MICAL2 negative, black arrow), MICAL2 expression in cardiomyocytes (I). Interestingly, in the border zone (J) some capillaries showed very low MICAL2 expression (red arrow) while others were negative (black arrow).
Magnification: 2.5×, in A, B, scale bar: 200 μm; 40× in C-J, scale bar: 10 μm.

5, time-lapse movies of WHAs). Serum deprivation (indicated as 'Starv' in figures) significantly reduced motility of reference cells that however recovered partially (about 50%) when stimulated with VEGF, whereas M2KD cells did not (Fig. 5A).

A chemotaxis assay showed a reduction of about 30% of M2KD cell response to VEGF stimulation (Fig. 5B).

The functional response was mirrored by F-actin redistribution upon VEGF stimulation (70 ng/ml, 30 min), as shown by staining (Fig. 5C–J). VEFG stimulation promoted the reorganization of F-actin filaments in CTR cells (Fig. 5E, F). The remodeling was completely undetectable in M2KD cells (Fig. 5I–J). Analysis of the F-actin fluorescence intensity profile showed considerably higher amplitude and number of peaks corresponding to stress fibers in Starved CTR (Fig. 5C and K) compared to Starved KD (Fig. 5G and L) cells.

Altogether these data suggest that post-transcriptional inhibition of MICAL2 expression, affecting F-actin remodeling, hinders adhesion and

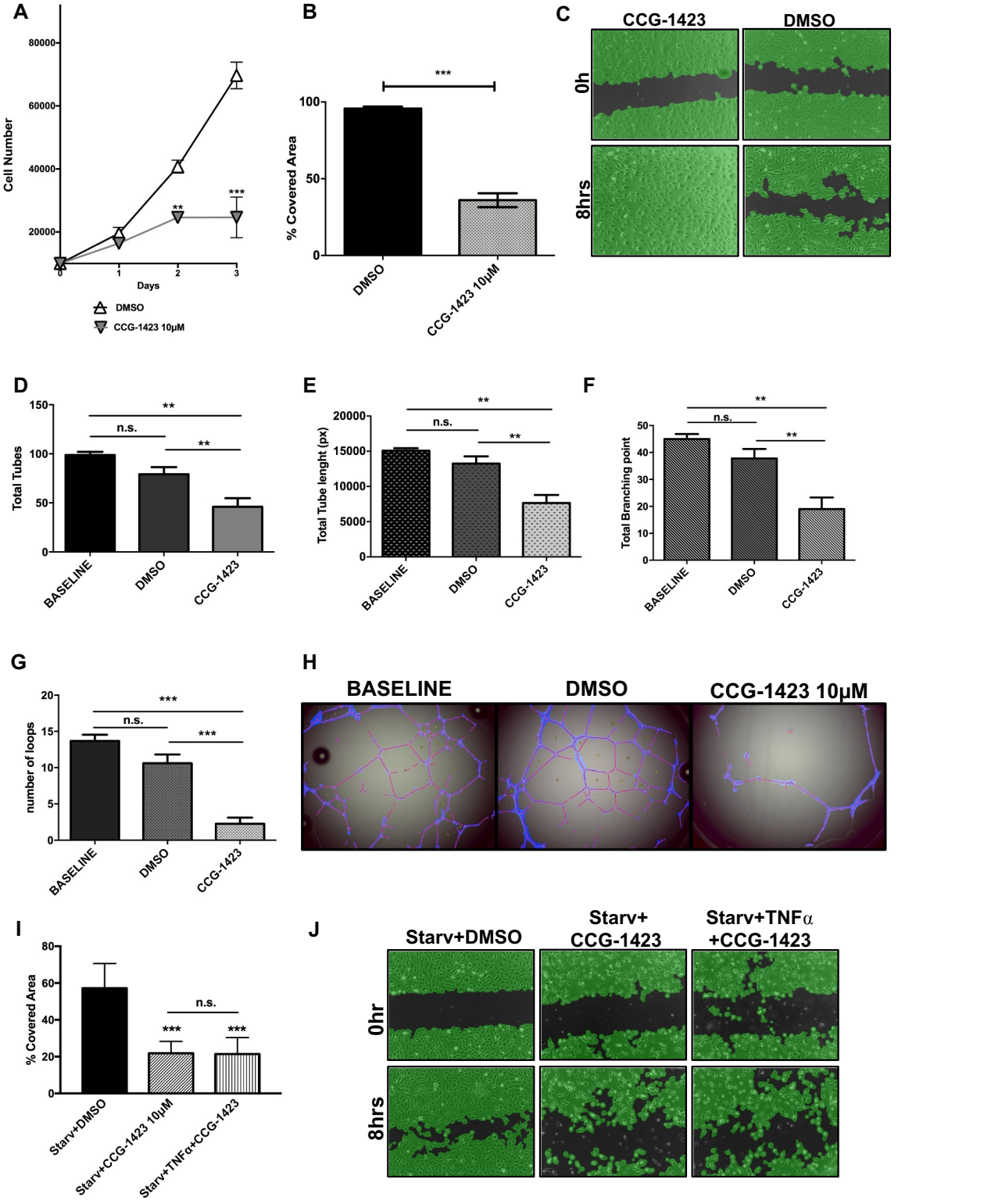

(caption on next page)

Fig. 3. Direct inhibition of MICAL2 with CCG-1423 reduces functional properties of activated endothelial cells *in vitro*.
CCG-1423 is an inhibitor of SRF/MRTF-A pathway through direct binding of MICAL2. It was tested on HMEC-1 cells exposed to 1) complete medium containing 10% FBS (identified as 'Baseline' in D-H); 2) starvation, serum-free medium (Starv); 3) Starv medium +10 ng/μl TNF-alpha; 4) Starv medium +0.1% DMSO; 5) Starv medium +10 μM CCG-1423; 6) Starv medium +10 ng/μl TNF-alpha +10 μM CCG-1423. We also tested 5 μM CCG-1423, without measurable effect on HMEC-1 cell viability (see Supplementary Fig. ~~6~~ 3).
A: Cell proliferation was found 70% reduced after a three-day treatment (Student's *t*-test for unpaired samples; $_{**}p < 0.01$, $_{***}p < 0.001$).
B: 2D migration upon treatment in an 8-h WHA was 60% reduced (Student's t-test for unpaired samples; $_{***}p < 0.001$).
C: representative result of WHA (magnification: 10×).
Morphology parameters of tube formation were also evaluated upon treatment with 10 μM CCG-1423. One-way ANOVA and Bonferroni Multiple Comparison post-hoc test revealed a significant reduction of total tubes number (D), of total tube length (E), total branching points (F) and of loop number (G). $^{**}p < 0.01$, $^{***}p < 0.001$.
H: a representative result of a 20-h tube formation on Geltrex (Thermo Fisher Scientific). Magnification: 5×.
I: 2D migration was significantly reduced by 10 μM CCG-1423 on ECs activated by a pre-treatment with 10 ng/μl TNF-alpha in serum-free medium (Starv), One-way ANOVA; $_{***}p < 0.001$.
All data are means ± SEM. Experiments were repeated at least three times.
J: representative result of an 8-h WHA. Magnification: 10×.
All images were acquired with a 12-bit AxioCam MRc camera (Zeiss) connected to a Zeiss Axioskop 40 (Zeiss) microscope and Zeiss objective using the AxioVision (Zeiss) software.
Image analysis was performed with Tube Formation Image Analysis Platform and Wound Healing Image Analysis Platform software (Wimasis).
All experiments were repeated more than three times.

motility of ECs and reduces viability *in vitro*. Abating MICAL2 impedes capillary EC response to VEGF, a most critical endothelial growth factor.

Image acquisition: Leica TCS-NT confocal microscope (Leica) equipped with argon-krypton laser. Magnification: 40×.

F-actin analysis was performed with ImageJ 1.50i software on several fields as those represented by yellow squares in C and G, by plotting the fluorescence intensity profile along a straight selection line (in yellow) of about 16 μm perpendicular to stress fibers main axis. K: SVEC4-10 CTR. L: SVEC4-10 KD.

3.5. Transcriptome analysis indicates a role for MICAL2 in regulating angiogenic gene expression pathways

We performed a genome-wide gene expression analysis using Affymetrix arrays to analyze the transcriptional profiles induced by M2KD in SVEC4–10 cells. Results were analyzed with Gene Ontology (GO) and Gene Set Enrichment Analysis (GSEA) algorithms to perform enrichment analysis on gene sets. We found 465 up-regulated and 672 down regulated unique gene symbols (Fig. 6A, Supplementary Table 2). To validate these results, we performed qRT-PCR analysis on some highly affected genes (Cd34, FC: +5,7; Hoxa9, FC: −2,4) and results were coherent (Supplementary Fig. ~~5~~ 6).

GO analysis indicated that M2KD affected a total of 49 Biological Processes (BPs, Supplementary Table 3), among which those regulating the circulatory system development, angiogenesis, inflammatory response, response to cytokines, regulation of reactive oxygen species, and cell adhesion. The most relevant include "Angiogenesis", "Cell adhesion", "Response to cytokine", "Inflammatory response" and "Vasculature development", "Cell differentiation" (Fig. 6B, expressed as the -log10(q-value). Benjamini test was used as multiple testing correction technique to globally correct enrichment *p*-values. Only the terms that had significant p-values ($p < 0.05$) after the corrections were considered.

GSEA functional enrichment of differential genes identified 30 activated and 101 de-activated pathways (FDR < 0.25; Supplementary Table 4) in M2KD cells. The top 30 significant activated and de-activated gene sets are shown in Fig. 6C, D. Interestingly, pathways involved in angiogenesis, cell adhesion, cell matrix adhesion, cell cycle, NOTCH signaling, and immune response were deactivated in M2KD cells. In turn, pathways involved in cell death, hypoxia response and reactive oxygen species production were activated.

We explored the associations between these genes on a global scale using the Network connectivity identification by StringApp and Cytoscape analysis and found a main network of 150 proteins with at least one interaction (Fig. 6E). Successively, Cluster One algorithm identified six significant modules of highly connected proteins with similar function within the main network (Fig. 6F).

Altogether, these results support our *in vivo* and *in vitro* observations suggesting that Mical2 is activated in response to microenvironmental signals during physio-pathological neo-angiogenesis and plays a crucial role in different phases of the angiogenic process in post-natal endothelium. Characterizing the interaction among these gene products will better decipher the role of the gene on EC biology.

4. Discussion

In previous work we observed that MICAL2 was over-expressed in cancer cells of aggressive, metastatic human cancers [14], whereas cancer cells of more differentiated, less aggressive tumors were MICAL2 negative. In this work, we observed that regardless of MICAL2 expression in cancer cells, MICAL2 was always expressed by ECs of their neo-angiogenic capillaries. Neo-angiogenesis is a complex, multistep process in which several humoral and structural factors are activated/re-activated to allow sprouting of novel capillary blood vessels from pre-existing vasculature. The last four decades of studies in the field of anti-angiogenic, co-adjuvant therapy of cancer have led to three main advancements which are also areas of potential improvement: i) an increased molecular understanding of tumor angiogenesis, which is fundamental to acquire new tools for anti-angiogenic gene therapy; ii) more efficient targeting of cancer-associated ECs, which, being more genetically stable, may actually be preferable targets over cancer cells. In addition, the same anti-angiogenic drug may be efficient also against cancer cells [26,27]; iii) more specific gene-delivery strategies, to allow specific targeting of cancer and cancer-associated cells with respect to normal tissues [7].

In this work, we report three key findings: 1) MICAL2 is expressed in pathological neo-angiogenic ECs but not in normal capillaries and ECs of normal blood vessels (Figs. 1, 2); 2) pharmacological inhibition and KD of MICAL2 expression reduce EC viability and functional performance (Figs. 3–5); 3) M2KD ECs no longer respond to VEGF stimulation *in vitro* (Fig. 5).

These observations suggested the hypothesis of a link between MICAL2 expression and pathological neo-angiogenesis induced by inflammation (schematized in Fig. 7). We tested the hypothesis in a relevant physio-pathological animal model that is neo-angiogenesis induced by ischemia in the heart. Myocardial, post-ischemic neo-angiogenesis, although of controversial significance for patient outcome, shows a molecular landscape very similar to tumor-associated neo-angiogenesis [25]. Consistently, in the rat ischemic heart MICAL2

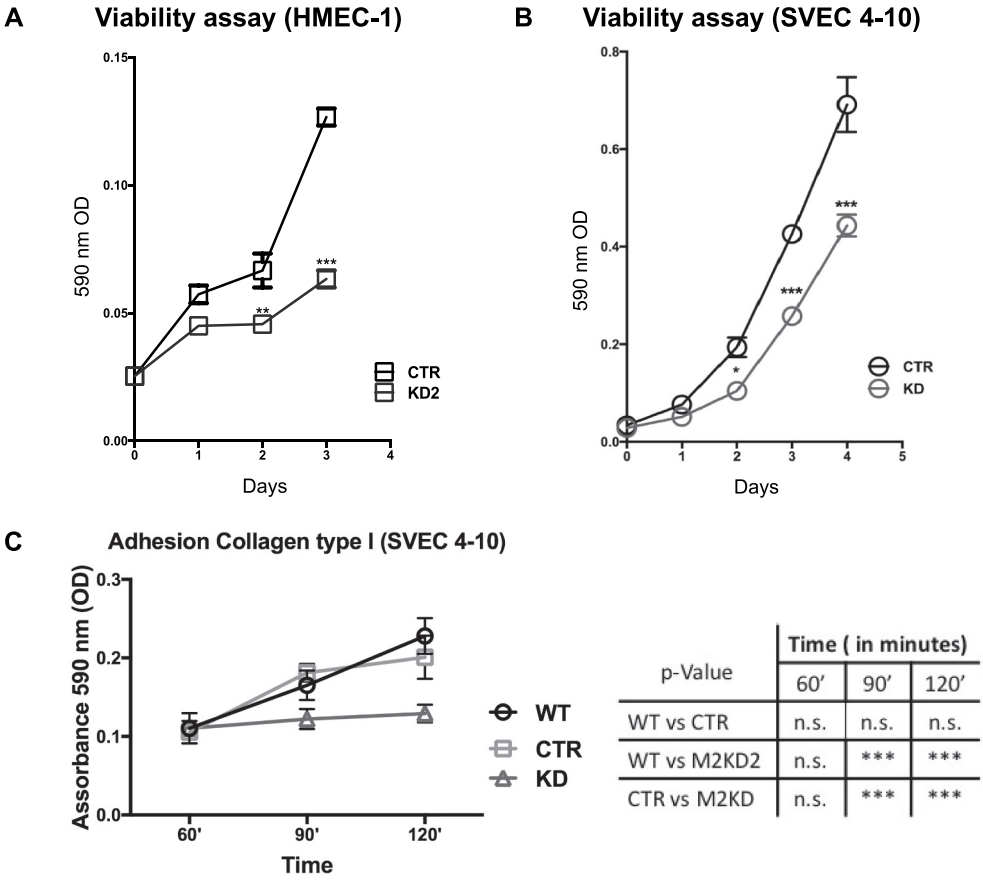

p-Value	Time (in minutes)		
	60′	90′	120′
WT vs CTR	n.s.	n.s.	n.s.
WT vs M2KD2	n.s.	***	***
CTR vs M2KD	n.s.	***	***

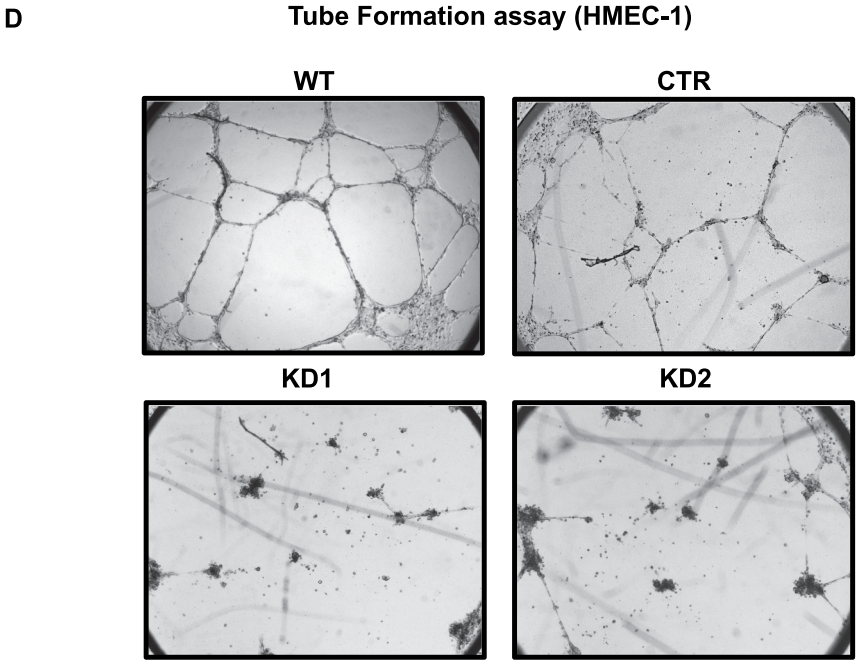

Fig. 4. MICAL2 loss of function reduces human and murine endothelial cells viability and hampers adhesion and functional properties *in vitro*.

MICAL2 gene expression was knocked-down in human HMEC-1 and murine SVEC4–10 cells with gene-specific shRNA-expressing plasmids. Mixed populations of stably expressing cells were selected with G418. Cell viability was measured for several days with MTT assay. Student's *t*-test for unpaired samples showed a reduction of about 50% of OD at 590 nm in HMEC-1 cells after three days (A) and in SVEC-4–10 after four days (B). The experiments were repeated at least three times, each time with three replicas. All data are means ± SEM; $_{*}p < 0.05$, $_{**}p < 0.01$, $_{***}p < 0.001$.

Cell adhesion was measured at different time points in M2KD SVEC4–10, seeded on collagen type I (C). One-way ANOVA test showed a statistically significant difference of adhesion by KD cells already at 90 min after seeding, and even more at 120 min. Experiments were repeated at least three times, each time with three replicas. All data are means ± SEM. ($_{***}p < 0.001$).

D: M2KD HMEC-1 cells showed a dramatic difference in their ability to form tubes on Geltrex in TFA, a most widely used *in vitro* assay to model the reorganization stage of angiogenesis and study rapidly and quantitatively genes or pathways involved in the process. 20 h from seeding in complete medium, neither KD1 nor KD2 had been able to form tubes, which were well detectable in reference samples (WT and CTR cells). Magnification: 5×.

was found in ECs of new capillaries, while it was absent from stable vessels of larger caliber, or from same-size capillaries of the remote zone (*i.e.* not affected by the post ischemic neo-angiogenic event). In the border zone (the region between the healthy and the ischemic tissue), MICAL2 stain was quite peculiar: some capillaries were negative, some adjacent ones showed a weak staining, as if in this region some capillaries had been activated by the nearby inflammatory process while some others not quite.

The previous observations suggested that MICAL2 over-expression was caused by signals in the cancer niche able to activate ECs. It is well known that tissue hypoxia induces diffuse inflammation and immune-driven angiogenesis, with different leukocyte subtypes that condition the microenvironment producing angiogenic factors, interleukins and proteases. Moreover, the strong MICAL2 expression increase in

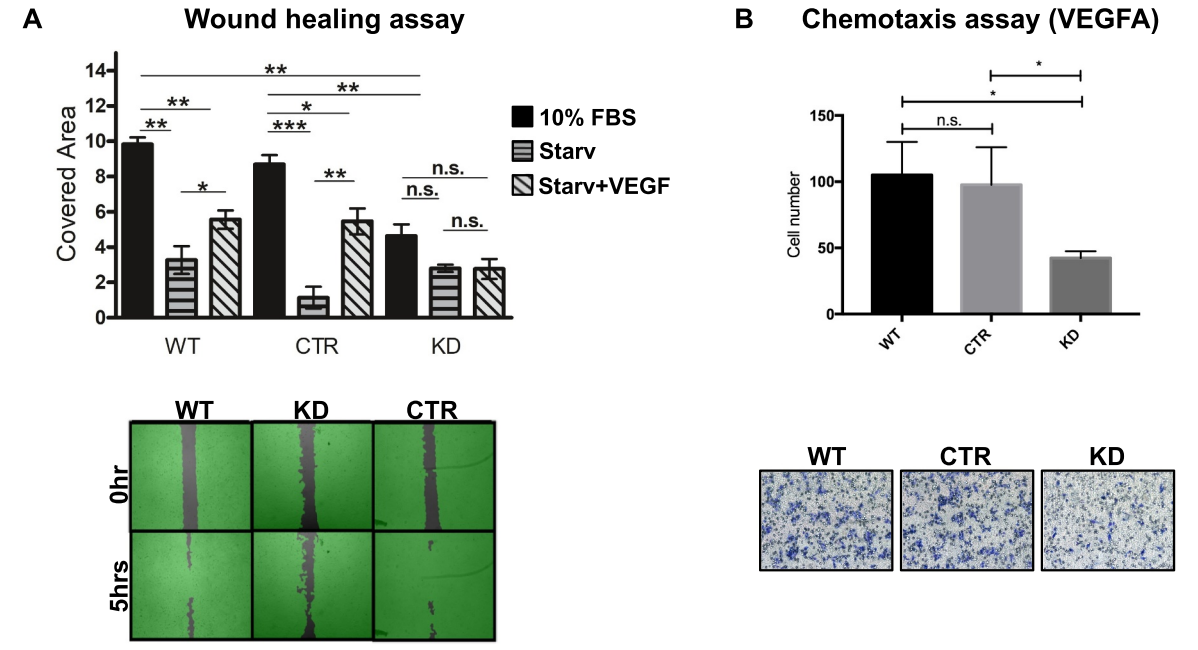

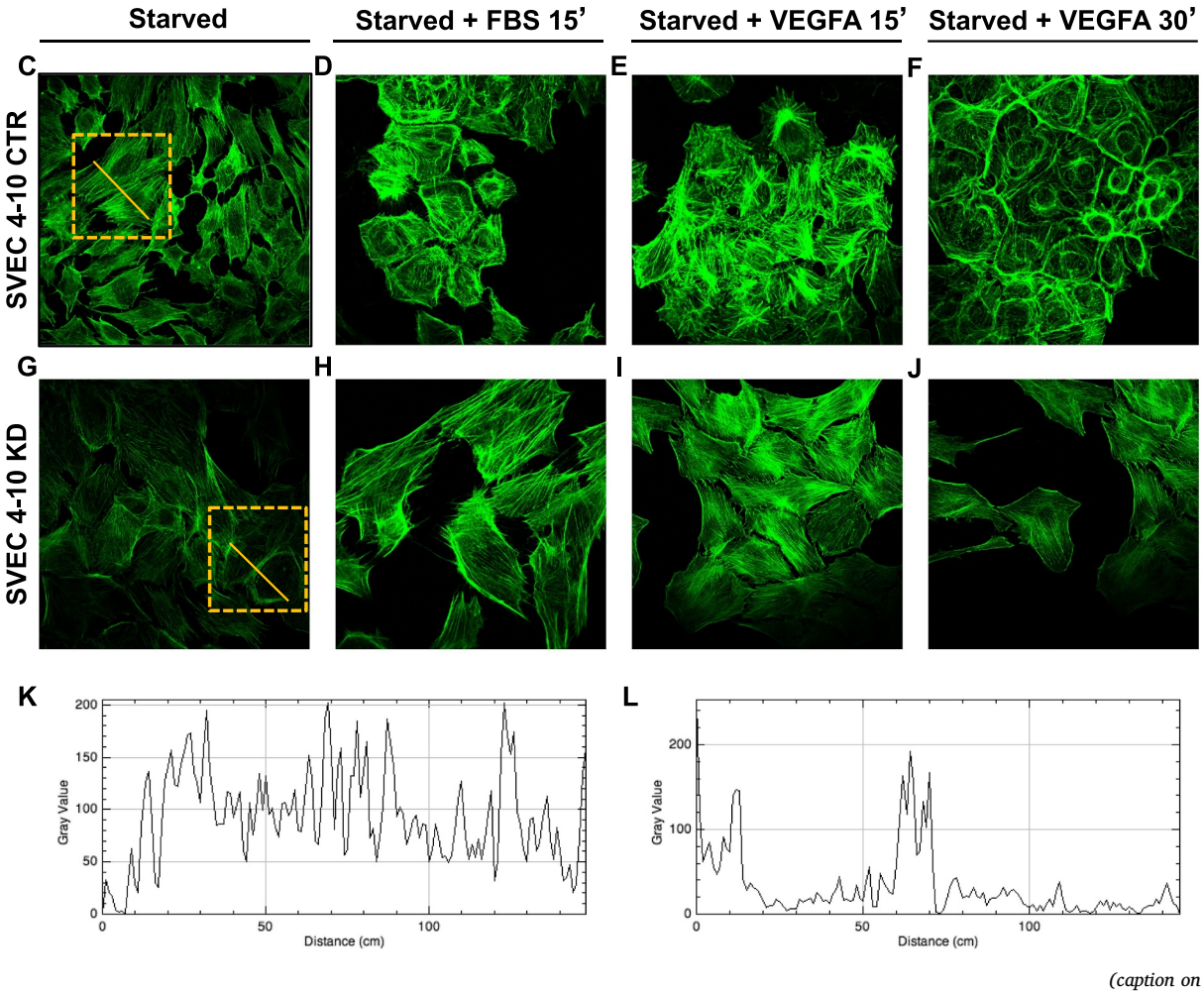

(caption on next page)

Fig. 5. Response of endothelial cells to VEGF stimulation is strongly reduced by MICAL2 knock-down.
A: All cell types in serum-free medium (Starv) slowed down in 5-h WHA without any statistically significant difference among them. WT and CTR cells partially recovered after 70 ng/ml VEGF administration; M2KD cells were insensitive. Graph: area covered during the test (masked in green in the panel below; experiment in complete medium) measured in arbitrary units. Image analysis: Wound Healing Image Analysis Platform software (Wimasis). Magnification: 5×.
B: Chemotaxis assay performed with Boyden chamber. 8000 cells were seeded in the upper wells. The lower wells contained serum-free cell medium with or without 70 ng/ml VEGF. After 8 h at 37 °C, the membrane (8 μm-pore, polycarbonate, Neuro Probe, Inc.) was removed and stained with Diff-Quick (Medion Diagnostics). Graph: number of cells that crossed the membrane during the assay. Lower panel: representative cases. Magnification: 5×. Images analysis: Cell Counter Plug In, ImageJ suite.
All data are means ± SEM. All experiments were repeated at least three times, each time with three replicas; One-way ANOVA test, * $p < 0.05$, ** $p < 0.01$, *** $p < 0.001$.
SVEC4–10 cells were starved (C: CTR; G: KD) then stimulated with 70 ng/ml VEGF. Fixed after 15 min (E: CTR, I: KD) and 30 min (F: CTR, J: KD), CTR cells featured large, subcortical F-actin rings, while F-actin remodeling was undetectable in M2KD cells, which showed unchanged stress fibers in VEGF-treated and untreated condition alike. For comparison, cells were stimulated with 10% FBS for 15 min (D: CTR, H: KD).

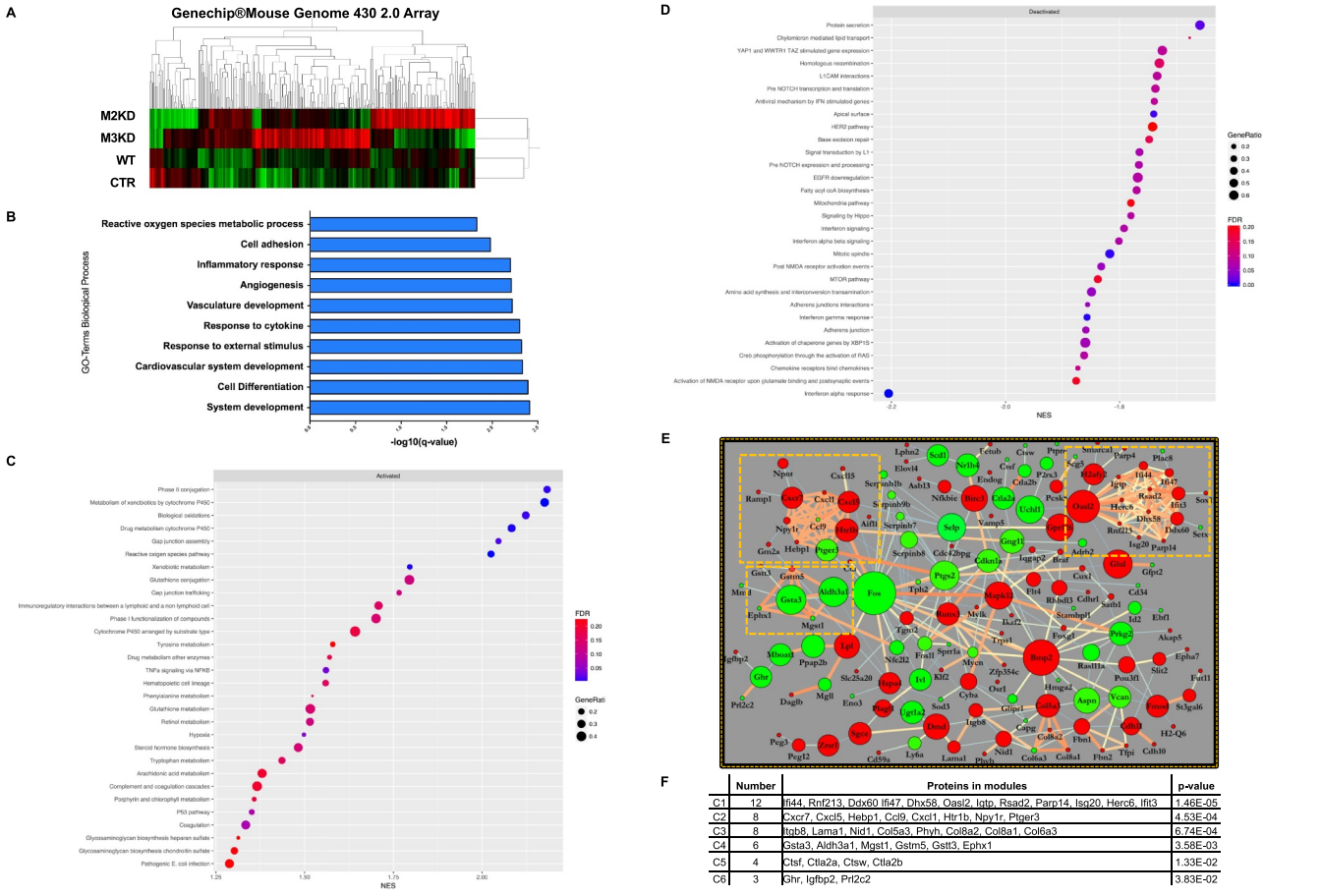

	Number	Proteins in modules	p-value
C1	12	Ifi44, Rnf213, Ddx60 Ifi47, Dhx58, Oasl2, Igtp, Rsad2, Parp14, Isg20, Herc6, Ifit3	1.46E-05
C2	8	Cxcr7, Cxcl5, Hebp1, Ccl9, Cxcl1, Htr1b, Npy1r, Ptger3	4.53E-04
C3	8	Itgb8, Lama1, Nid1, Col5a3, Phyh, Col8a2, Col8a1, Col6a3	6.74E-04
C4	6	Gsta3, Aldh3a1, Mgst1, Gstm5, Gstt3, Ephx1	3.58E-03
C5	4	Ctsf, Ctla2a, Ctsw, Ctla2b	1.33E-02
C6	3	Ghr, Igfbp2, Prl2c2	3.83E-02

Fig. 6. Analysis of genome-wide gene expression profile.
A: Heatmap of gene expression profile. Clusters reveal a rather distinct effect of M2KD compared to M3KD in terms of up (red) and down (green) regulation of gene expression. This is interesting also considering that MICAL3 expression was not evident in cancer-associated ECs [14], suggesting MICAL family members exert different roles in endothelial homeostasis.
B: GO functional annotation of up and down regulated genes in M2KD cells was performed using the Database for Annotation, Visualization and Integrated Discovery (DAVID; https://david.ncifcrf.gov/) setting a p-value < 0.05 on the Biological Process (BP) GO terms.
Dot plot of the top 30 activated (C, normalized enrichment score NES > 0) and deactivated (D, normalized enrichment score NES < 0) gene sets from the Preranked Gene Set Enrichment Analysis in the M2KD cells. Dot color indicates statistical significance of the enrichment; dot size represents the fraction of genes annotated to each term. Gene sets are ranked in decreasing order based on the NES value. FDR: false discovery rate; NES: normalized enrichment score.
E: Protein networks activated in Mical2 KD cells built with the StringApp (Search Tool for the Retrieval of Interacting Genes/Proteins) [24].
F: Cluster One algorithm identified six significant modules of highly connected proteins with similar function in the main network. The 12 genes listed in Cluster 1 are involved in the immune response process and all of them were down regulated in M2KD cells. Cluster 2 counted eight protein components of G-protein coupled receptor signaling pathway involved in the response to cytokine and chemotaxis. Cluster 3 consisted of six genes involved in biological adhesion and in extracellular matrix organization and all of them, except Col6a3, were down regulated in M2KD cells. Red: down regulation; green: up regulation.

response to TNF-alpha stimulation *in vitro* (Supplementary Fig. 2) suggested that indeed the gene transcriptional activation is susceptible to pro-angiogenic, pro-tumor signaling presented by inflammation in cancer tissue.

In post-natal life, the majority of processes involving angiogenesis are in fact strictly related to inflammation, both in physiological and pathological conditions. Neo-angiogenesis in the tumor microenvironment, as well as in the ischemic myocardial tissue, is characterized by the release of many pro-inflammatory cytokines such as TNF-alpha and others, and by hypoxia, *per sé* a common denominator for angiogenesis

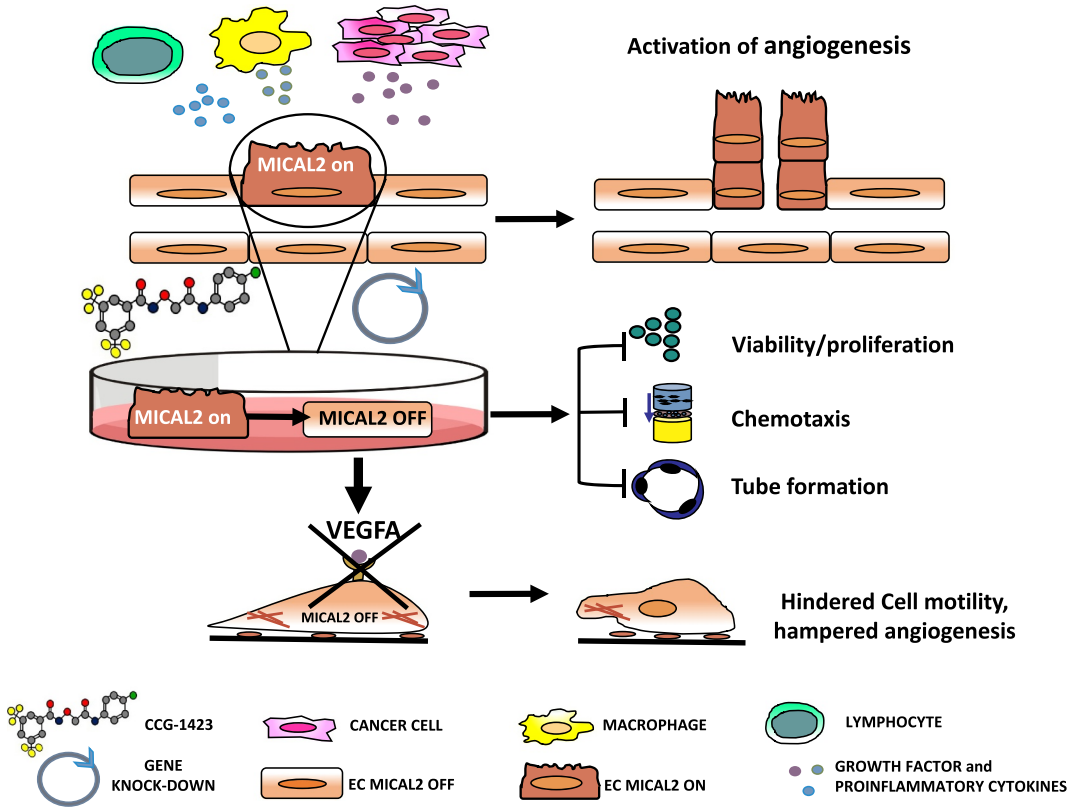

Fig. 7. A model for MICAL2 role in neo-angiogenesis.

and inflammation. The molecular mechanism unifying the regulation of the hypoxia response in terms of neo-angiogenesis and inflammatory reaction involves two main transcription factors, *i.e.* nuclear factor kappa B (NF-kappa B) and hypoxia-inducible factors (HIFs). Accordingly, a preliminary *in silico* analysis of MICAL2 putative promoter region (Eukaryotic promoter database, EPD; PROMO) indicated the presence of several predicted binding sites for both NF-kappa B and HIF1 transcription factors (observations not shown).

Further, in all human and experimental lesions, we observed abundant cells morphologically identified as inflammatory infiltrates, showing strong MICAL2 staining (Fig. 1J, M; Fig. 2E). Certainly, the neo-angiogenic process at ischemic sites can be additionally enhanced by reciprocal stimulation of ECs and monocytes/macrophages owing to their production of angiogenic molecules [28]. Possibly, MICAL2-expressing cells of immune origin further promote the pro-angiogenic cancer niche, therefore representing another reason to abate MICAL2 in this context.

Specific pharmacological inhibition of MICAL2 with CCG-1423 reduced cell viability and 2D motility significantly (Fig. 3). In TFA, ECs attempted to form connections that were not stable and rapidly regressed to leave only abortive, sparse tubes and practically no nets on Matrigel (Fig. 3).

Similarly, MICAL2 gene abatement, although not complete (Supplementary Fig. 1), significantly reduced both human and murine EC viability (Fig. 4), and significantly impaired EC adhesion and tube formation (Figs. 4, 5).

Consistent with previous reports showing that Semaphorin3A requires MICAL2 to mediate VEGF biological function in a mouse model of brain ischemia [19], our data also demonstrated that MICAL2 is essential for VEGF response in ECs (Fig. 5). This result is important in the context of cancer studies because the VEGF signaling system, essential for angiogenesis, is the direct or indirect target of most current anti-angiogenic therapies. These therapies are not free of adverse side effects, thereby motivating the search for new potential pharmacological targets.

In normal, stable blood vessels MICAL2 is not expressed in endothelium, but in VSMC (Fig. 2F). So, although the problem of a correct delivery has yet to be tackled, MICAL2 differential expression between normal and cancer-associated capillaries is a positive asset in view of potential therapeutic applications.

Our observation regarding VEGF refractoriness of M2KD cells finds support in literature showing MICAL2 as part of the p130Cas interactome activated by VEGF stimulation, which MICAL2 enters with a delayed (> 10 min) and persistent (> 60 min) interaction with p130Cas, together with other regulators of actin filament assembly [20], thereby suggesting a role for MICAL2 in rather late angiogenesis events.

Further, GSEA transcriptome analysis of M2KD cells showed that, among other pathways, the 'Angiogenesis' gene set was down regulated, reinforcing the hypothesis of a possible role for MICAL2 in the process (Supplementary Table 4). The concomitant down regulation of the 'Apical surface' genes, *i.e.* genes encoding proteins important for cell polarity (apical area), suggested that MICAL2 might participate as a polarity gene. Interestingly, MICAL2 abatement affected the expression of genes relevant to the formation of cell-cell-contact, as suggested by the up-regulation of 'Gap junction assembly' and 'Gap junction trafficking' gene sets, and the concomitant down regulation of 'Adherens junction' and 'Adherens junction interactions' gene sets.

Cell polarization is in itself a multistep process with interplay between the coordinated assembly of tight junctions and adherens junctions with several other cell activities such as cytoskeleton reorganization, redistribution of organelles and membrane traffic. Indeed, a clear role in this process has been defined previously for other members of the MICAL family. In fact, the MICAL-Like2 protein is necessary to coordinate the assembly of tight and adherens junctions through interaction with Rab8 and Rab13 proteins [29]. The MICAL2 protein was excluded to have a role in this physical interaction, however our gene expression study suggested an involvement in controlling

the expression of genes both in the 'Adherens junction' and 'Apical junction' sets. Together with down regulation of the *Cdh11* gene (Supplementary Table 4) and reduced adhesion to the matrix (Fig. 4C), this dual involvement might explain the results of TFA in M2KD cells where we observed initial formation of tubular primordia, possibly thanks to early type of cell-cell junction, that later failed to stabilize and regressed under the establishment of intracellular traction forces, unlike in the WT cells (Fig. 4D). Interestingly, our data are coherent with observations that cells treated with a gap-junction inhibitor enhanced the formation of F-actin and focal adhesions [30]. Indeed, M2KD transcriptome suggested that gap junction gene expression increases (Supplementary Table 4) concomitantly with strong reduction of F-actin stress fibers (Fig. 5).

In addition, it cannot go unnoticed that also the 'Yap1 and Taz stimulated gene expression' and the 'Signaling by Hippo' gene sets resulted deactivated (Supplementary Table 4). This is particularly interesting in light of recent observations showing that YAP/TAZ are activated and transferred to the nucleus of cancer-associated, neoangiogenenic ECs, and that VEGF-mediated cytoskeletal actin modification is necessary to allow such translocation [31]. It is tempting to speculate, although it should be experimentally verified, that MICAL2 activity might be localized in the stream of signal directed from VEGF-mediated cytoskeletal modification to YAP/TAZ nuclear translocation and subsequent activation of downstream gene expression events. In M2KD cells, this stream of signaling is likely hampered due to block/reduction of actin modification, therefore rendering MICAL2 mechanistically responsible of the deactivation of the 'YAP/TAZ stimulated' gene set observed in our study.

4.1. Conclusion

This work, for the first time describes the expression of MICAL2 in neo-angiogenic endothelium and a role for the protein in EC viability and function, posing MICAL2 within a direct, mechanistic correlation between cancer microenvironment factors (such as hypoxia and inflammatory cytokines) and redox modification of cytoskeletal dynamics. While these are significant findings because stress a growing relevance of MICAL2 to human cancer, it is worth mentioning that a small-molecule inhibitor of MICAL2 already exists.

As shown by the genome-wide transcription study of KD cells, Mical2 is a multifunctional protein that participates in at least 49 different biological processes, somewhat not surprising from a protein involved in modifying F-actin. However, for the relevance to this work, we stress here that the GO terms 'Angiogenesis', 'Vascular development' and 'Cardiovascular system development' were recognized in a group of ten biological processes. Also, we showed that pharmacological inhibition of MICAL2 enzymatic activity and gene KD converged both on markedly reducing ECs angiogenic properties. On these bases, we suggest that MICAL2 inhibition could be beneficial in cancer- and non-cancer-associated neo-angiogenesis associated to chronic tissue inflammation.

Our present data from *in vivo* and *in vitro* observation suggest collectively that MICAL2 is involved in neo-angiogenesis mediating VEGF signaling in human and murine capillary ECs activated by inflammatory stimulation. Analysis of a larger number of patients will tell whether MICAL2, as a marker of endothelial activation, also represents a new prognostic marker for neo-angiogenesis. Together with our previous results [14], present data also suggest that being MICAL2 expressed both in cancer cells and cancer -associated ECs, it may represent a target for a therapeutic tool oriented both against cancer cells and neo-angiogenic ECs [33,34].

Supplementary data to this article can be found online at https://doi.org/10.1016/j.bbadis.2019.04.008.

Transparency document

The Transparency document associated with this article can be found, in online version.

Acknowledgements

The authors thank Dr. Claudia Kusmic and Dr. Gualtiero Pelosi (Institute of Clinical Physiology, National Research Council, Pisa, Italy) for kind gift of histological sections of rat ischemic hearts and for histopathological evaluation; Dr. Antonio Giuseppe Naccarato (U.O.C. Anatomia Patologica, Azienda Ospedaliera Universitaria Pisana, Pisa, Italy) for human glioblastoma sections.

Many thanks also to little Riccardo M. Andreazzoli, he knows what for.

Funding

The project was supported by Istituto Toscano Tumori (now ISPRO), Regione Toscana, Italy; DA is also truly grateful to Lions Club International, District 108LA, Toscana, Italy, in particular to Carlo Bianucci and Giovanna Ciampi, and to the following Clubs: Fiesole, Firenze Amerigo Vespucci, Firenze Arnolfo di Cambio, Firenze Brunelleschi, Firenze Cosimo de' Medici, Firenze Poggio Imperiale, Firenze Ponte Vecchio, Poggio a Caiano, Prato Curzio Malaparte; to Mr. and Mrs. Rosario Leonardis, to Mr. and Mrs.Vito Mingolla, and to the Associazione Nazionale Incursori Esercito (A.N.I.E., Livorno, Italy) for their generous and enthusiastic support of the study.

Availability of data and material

The datasets supporting the conclusions of this article are included within the article and its additional files. Raw data are available at Gene Expression Omnibus under accession number GSE120494.

All material in the study is available upon request.

Authors' contributions

DA designed the study, coordinated the work, provided funds and wrote the manuscript; IB, SM, and ET performed all experiments; AP, CA, and MCM collected tissue samples and clinical data; FS and CDC provided experimental support; DA, IB, SB, ET, and GB analyzed and interpreted the data; MV and LP provided new reagents; MC performed time lapse movies; DA and IB drafted the manuscript and prepared the illustrations. All authors read and approved the final manuscript.

Ethics approval and consent to participate

The study was done in accordance with the Declaration of Helsinki. All patients gave informed written consent. All protocols either involving human subjects or animal studies were approved by from local ethic committees.

Consent for publication

All contributing authors agree to the publication of this article.

Competing interests

None to declare.

References

[1] D. Hanahan, R.A. Weinberg, Hallmarks of cancer: the next generation, Cell. 144 (2011) 646–674, https://doi.org/10.1016/j.cell.2011.02.013.
[2] S. Seaman, J. Stevens, M.Y. Yang, D. Logsdon, C. Graff-Cherry, B. St Croix, Genes

that distinguish physiological and pathological angiogenesis, Cancer Cell 11 (2007) 539–554, https://doi.org/10.1016/j.ccr.2007.04.017.
[3] W.C. Aird, Molecular heterogeneity of tumor endothelium, Cell Tissue Res. 335 (2009) 271–281, https://doi.org/10.1007/s00441-008-0672-y.
[4] D. Huang, H. Lan, F. Liu, S. Wang, X. Chen, K. Jin, et al., Anti-angiogenesis or pro-angiogenesis for cancer treatment: focus on drug distribution, Int. J. Clin. Exp. Med. 8 (2015) 8369–8376.
[5] J. Folkman, E. Merler, C. Abernathy, G. Williams, Isolation of a tumor factor responsible for angiogenesis, J. Exp. Med. 133 (1971) 275–288.
[6] F. Bertolini, Biomarkers for angiogenesis and antiangiogenic drugs in clinical oncology, Breast 18 (2009) S48–S50, https://doi.org/10.1016/S0960-9776(09)70272-3.
[7] R.Y. Kiseleva, P.M. Glassman, C.F. Greineder, E.D. Hood, V.V. Shuvaev, V.R. Muzykantov, Targeting therapeutics to endothelium: are we there yet? Drug Deliv. Transl. Res. 8 (2018) 883–902, https://doi.org/10.1007/s13346-017-0464-6.
[8] R. Pasqualini, W. Arap, D.M. McDonald, Probing the structural and molecular diversity of tumor vasculature, Trends Mol. Med. 8 (2002) 563–571.
[9] P.-P. Wong, N. Bodrug, K.M. Hodivala-Dilke, Exploring novel methods for modulating tumor blood vessels in cancer treatment, Curr. Biol. 26 (2016) R1161–R1166, https://doi.org/10.1016/j.cub.2016.09.043.
[10] S. Loges, T. Schmidt, P. Carmeliet, Mechanisms of resistance to anti-angiogenic therapy and development of third-generation anti-angiogenic drug candidates, Genes Cancer 1 (2010) 12–25, https://doi.org/10.1177/1947601909356574.
[11] J.R. Terman, T. Mao, R.J. Pasterkamp, H.-H. Yu, A.L. Kolodkin, MICALs, a family of conserved flavoprotein oxidoreductases, function in plexin-mediated axonal repulsion, Cell. 109 (2002) 887–900.
[12] R.-J. Hung, U. Yazdani, J. Yoon, H. Wu, T. Yang, N. Gupta, et al., Mical links semaphorins to F-actin disassembly, Nature. 463 (2010) 823–827, https://doi.org/10.1038/nature08724.
[13] R.-J. Hung, C.W. Pak, J.R. Terman, Direct redox regulation of F-actin assembly and disassembly by Mical, Science. 334 (2011) 1710–1713, https://doi.org/10.1126/science.1211956.
[14] S. Mariotti, I. Barravecchia, C. Vindigni, A. Pucci, M. Balsamo, R. Libro, et al., *MICAL2* is a novel human cancer gene controlling mesenchymal to epithelial transition involved in cancer growth and invasion, Oncotarget. 7 (2014) 1808–1825, https://doi.org/10.18632/oncotarget.6577.
[15] S. Ashida, M. Furihata, T. Katagiri, K. Tamura, Y. Anazawa, H. Yoshioka, et al., Expression of novel molecules, MICAL2-PV (MICAL2 prostate cancer variants), increases with high Gleason score and prostate cancer progression, Clin. Cancer Res. 12 (2006) 2767–2773, https://doi.org/10.1158/1078-0432.CCR-05-1995.
[16] J.R. Ho, E. Chapeaublanc, L. Kirkwood, R. Nicolle, S. Benhamou, T. Lebret, et al., Deregulation of Rab and Rab effector genes in bladder cancer, PLoS One 7 (2012) e39469, , https://doi.org/10.1371/journal.pone.0039469.
[17] Y. Wang, W. Deng, Y. Zhang, S. Sun, S. Zhao, Y. Chen, et al., MICAL2 promotes breast cancer cell migration by maintaining epidermal growth factor receptor (EGFR) stability and EGFR/P38 signalling activation, Acta Physiol. 222 (2018) e12920, , https://doi.org/10.1111/apha.12920.
[18] R. Hellweg, A. Mooneyham, Z. Chang, M. Shetty, E. Emmings, Y. Iizuka, et al., RNA sequencing of carboplatin- and paclitaxel-resistant endometrial cancer cells reveals new stratification markers and molecular targets for cancer treatment, Horm Cancer. 9 (2018) 326–337, https://doi.org/10.1007/s12672-018-0337-6.
[19] S.T. Hou, L. Nilchi, X. Li, S. Gangaraju, S.X. Jiang, A. Aylsworth, et al., Semaphorin3A elevates vascular permeability and contributes to cerebral ischemia-induced brain damage, Sci. Rep. 5 (2015) 7890, , https://doi.org/10.1038/srep07890.
[20] I.M. Evans, S.A. Kennedy, K. Paliashvili, T. Santra, M. Yamaji, R.C. Lovering, et al., Vascular endothelial growth factor (VEGF) promotes assembly of the p130Cas interactome to drive endothelial chemotactic signaling and angiogenesis, Mol. Cell. Proteomics 16 (2017) 168–180, https://doi.org/10.1074/mcp.M116.064428.
[21] E.W. Ades, F.J. Candal, R.A. Swerlick, V.G. George, S. Summers, D.C. Bosse, et al., HMEC-1: establishment of an immortalized human microvascular endothelial cell line, J. Invest. Dermatol. 99 (1992) 683–690.
[22] K.A. O'Connell, M. Edidin, A mouse lymphoid endothelial cell line immortalized by simian virus 40 binds lymphocytes and retains functional characteristics of normal endothelial cells, J. Immunol. 144 (1990) 521–525.
[23] M. Balsamo, I. Barravecchia, S. Mariotti, A. Merenda, C. De Cesari, M. Vukich, et al., Molecular and cellular characterization of space flight effects on microvascular endothelial cell function – preparatory work for the SFEF project, Microgravity Sci. Technol. 26 (2014) 351–363, https://doi.org/10.1007/s12217-014-9399-4.
[24] D. Szklarczyk, A. Franceschini, S. Wyder, K. Forslund, D. Heller, J. Huerta-Cepas, et al., STRING v10: protein-protein interaction networks, integrated over the tree of life, Nucleic Acids Res. (2015) D447–D452, https://doi.org/10.1093/nar/gku1003 43 Database issue.
[25] A. Szade, A. Grochot-Przeczek, U. Florczyk, A. Jozkowicz, J. Dulak, Cellular and molecular mechanisms of inflammation-induced angiogenesis, IUBMB Life 67 (2015) 145–159, https://doi.org/10.1002/iub.1358.
[26] L. Persano, M. Crescenzi, S. Indraccolo, Anti-angiogenic gene therapy of cancer: current status and future prospects, Mol. Asp. Med. 28 (2007) 87–114, https://doi.org/10.1016/j.mam.2006.12.005.
[27] T. Li, G. Kang, T. Wang, H. Huang, Tumor angiogenesis and anti-angiogenic gene therapy for cancer (review), Oncol. Lett. 16 (2018) 687–702, https://doi.org/10.3892/ol.2018.8733.
[28] P.R. Sanberg, D.-H. Park, N. Kuzmin-Nichols, E. Cruz, N.A. Hossne, E. Buffolo, et al., Monocyte transplantation for neural and cardiovascular ischemia repair, J. Cell. Mol. Med. 14 (2010) 553–563, https://doi.org/10.1111/j.1582-4934.2009.00903.x.
[29] R. Yamamura, N. Nishimura, H. Nakatsuji, S. Arase, T. Sasaki, The interaction of JRAB/MICAL-L2 with Rab8 and Rab13 coordinates the assembly of tight junctions and adherens junctions, Mol. Biol. Cell 19 (2008) 971–983, https://doi.org/10.1091/mbc.E07-06-0551.
[30] T. Okamoto, E. Kawamoto, Y. Takagi, N. Akita, T. Hayashi, E.J. Park, et al., Gap junction-mediated regulation of endothelial cellular stiffness, Sci. Rep. 7 (2017) 6134, , https://doi.org/10.1038/s41598-017-06463-x.
[31] X. Wang, A. Freire Valls, G. Schermann, Y. Shen, I.M. Moya, L. Castro, et al., YAP/TAZ orchestrate VEGF signaling during developmental angiogenesis, Dev. Cell 42 (2017) 462–478.e7, https://doi.org/10.1016/j.devcel.2017.08.002.
[32] M.R. Lundquist, A.J. Storaska, T.-C. Liu, S.D. Larsen, T. Evans, R.R. Neubig, et al., Redox modification of nuclear actin by MICAL-2 regulates SRF signaling, Cell. 156 (2014) 563–576, https://doi.org/10.1016/j.cell.2013.12.035.
[33] Y. Zhao, A.A. Adjei, Targeting angiogenesis in cancer therapy: moving beyond vascular endothelial growth factor, Oncologist. 20 (2015) 660–673, https://doi.org/10.1634/theoncologist.2014-0465.
[34] W. Ye, The complexity of translating anti-angiogenesis therapy from basic science to the clinic, Dev. Cell 37 (2016) 114–125, https://doi.org/10.1016/j.devcel.2016.03.015.